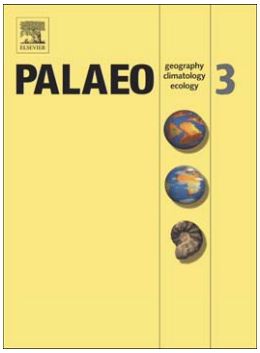

Changes in Timor Strait hydrology and thermocline structure during the past 130 ka

Elena Lo Giudice Cappelli, Ann Holbourn, Wolfgang Kuhnt, Marcus Regenberg

PII: S0031-0182(16)30466-7
DOI: doi: 10.1016/j.palaeo.2016.09.010
Reference: PALAEO 7983

To appear in: *Palaeogeography, Palaeoclimatology, Palaeoecology*

Received date: 24 February 2016
Revised date: 12 September 2016
Accepted date: 13 September 2016

Please cite this article as: Cappelli, Elena Lo Giudice, Holbourn, Ann, Kuhnt, Wolfgang, Regenberg, Marcus, Changes in Timor Strait hydrology and thermocline structure during the past 130 ka, *Palaeogeography, Palaeoclimatology, Palaeoecology* (2016), doi: 10.1016/j.palaeo.2016.09.010

Changes in Timor Strait hydrology and thermocline structure during the past 130 ka

Elena Lo Giudice Cappelli[1,2], Ann Holbourn[1], Wolfgang Kuhnt[1], and Marcus Regenberg[1]

[1]Institute of Geosciences, Christian-Albrechts-Universität zu Kiel, Ludewig-Meyn-Str. 14, 24118 Kiel, Germany.

[2]School of Geography and Geology, University of St Andrews, St Andrews, Fife Scotland, KY16 9AL, UK

Corresponding author: E. Lo Giudice Cappelli, (elgc@st-andrews.ac.uk)

Key Points

ITF thermocline flow intensified during MIS 5d-a and MIS 1

Local wet monsoon strengthened during early MIS 5e

Glacial thermocline warming reflects reduced ITF and advection of Indian Ocean waters

Abstract

Paleostudies of the Indonesian Throughflow (ITF) are largely based on temperature and salinity reconstructions of its near surface component, whereas the variability of its lower thermocline flow has rarely been investigated. We present a multi-proxy record of planktonic and benthic foraminiferal $\delta^{18}O$, Mg/Ca-derived surface and lower thermocline temperatures, X-ray fluorescence (XRF)-derived runoff and sediment winnowing for the past 130 ka in marine sediment core SO18471. Core SO18471, retrieved from a water depth of 485 m at the southern edge of the Timor Strait close to the Sahul Shelf, sits in a strategic position to reconstruct variations in both the ITF surface and lower thermocline flow as well as to investigate hydrological changes related to monsoon variability and shelf dynamics over time. Sediment winnowing demonstrates that the ITF thermocline flow intensified during MIS 5d-a and MIS 1. In contrast during MIS 5e, winnowing was reduced and terrigenous input increased suggesting intensification of the local wet monsoon and a weaker ITF. Lower thermocline warming during globally cold periods

(MIS 4 – MIS 2) appears to be related to a weaker and contracted thermocline ITF and advection of warm and salty Indian Ocean waters.

Keywords

Indonesian Throughflow, Timor Sea, lower thermocline, *Hoeglundina elegans* Mg/Ca, X-ray fluorescence core scanning.

1. Introduction

The Indonesian Throughflow (ITF) is a complex ocean current system that transports cool and fresh waters from the Pacific Ocean to the Indian Ocean and, thus, plays an important role in modulating local and global climate [*Cresswell et al.*, 1993; *Gordon and Fine*, 1996*; Gordon* 2005; *Oppo and Rosenthal* 2010]. The Timor Strait provides the main exit path for the ITF, as about half of the total transport (~7.5 Sv) takes place through this passage [*Sprintall et al*., 2009]. To date, our understanding of the past evolution of the ITF remains largely based on temperature and salinity reconstructions of its near surface component, down to ~200 m, whereas the variability of the lower thermocline component along the ITF pathway has rarely been investigated. The scarcity of investigations addressing past variability of intermediate and deep waters reflects to a large extent the difficulties in developing sensitive proxy recorders of temperature for the deeper ocean, where variations are generally more muted than at or close to the surface.

Based on a new Mg/Ca paleothermometry calibration study [*Lo Giudice Cappelli et al.*, 2015], we present the first Timor Strait record of lower thermocline temperatures spanning the last ~130 ka. We combine this benthic foraminiferal Mg/Ca data set from Core SO18471 with a multi-proxy record of planktonic and benthic foraminiferal $\delta^{18}O$, Mg/Ca-derived surface temperature and X-ray fluorescence (XRF)-derived runoff and sediment winnowing from the same core. The location of core SO18471 is strategic to reconstruct the variability of the ITF vertical structure over time, as it sits in a relatively shallow location, in a water depth of 485 m corresponding to the ITF lower thermocline flow, which allows to reconstruct the hydrological evolution of both surface and deeper water masses (Fig. 1). In addition, the proximity of core SO18471 to the Sahul Shelf allows monitoring of changes in sediment discharge and winnowing related to variations in the Indonesian-Australian Monsoon system and shelf dynamics over time. We compare our results with published isotope ($\delta^{18}O$) and Mg/Ca data from the Timor Sea to explore the regional variability in temperature and water mass properties and to assess the impact of glacial – deglacial sea level changes on regional hydrography.

2. Regional oceanography and climate dynamics

The Timor Sea encompasses the Timor Strait to the north and the Sahul Shelf to the south [*Cresswell et al.,* 1993]. The Timor Strait is dominated by the year-round southwestward flow of the ITF, while circulation on the Sahul Shelf strongly depends on the monsoon cycle [*Cresswell et al*., 1993; *Sprintall et al.,* 2009; *Schiller et al.,* 2011]. The ITF is driven across the Indonesian Archipelago by the pressure gradient between the tropical western Pacific and the Indian Ocean [*Cresswell et al.,* 1993] and consists of

surface to upper thermocline waters stemming from the North Pacific, and lower thermocline and intermediate waters of South Pacific origin [*Gordon and Fine*, 1996; *Talley and Sprintall*, 2005; *Sprintall et al*., 2009]. On their way to the Timor Strait, these water masses are intensely modified by tidal mixing [*Egbert and Ray*, 2001; *Ray et al.*, 2005; *Koch-Larrouy et al*., 2010], monsoon-driven upwelling [*Moore et al.*, 2003], and air-sea exchanges [*Wijffels et al.*, 2008] in the Banda Sea (Fig. 1) before entering the Indian Ocean [*Ffield and Gordon*, 1992; *Gordon and Susanto*, 2001; *Sprintall et al*., 2009].

Seasonal wind reversals linked to the Indonesian-Australian Monsoon system influence the circulation in the Timor Sea. During the austral summer monsoon (NW monsoon), the ITF and northeast currents on the Sahul Shelf are weaker because the pressure gradient between the Pacific and Indian Oceans is at its lowest [*Cresswell et al.*, 1993; *Sprintall et al*., 2009; *Schiller et al*., 2011]. As the Intertropical Convergence Zone (ITCZ) is in its southernmost position, Indonesia and NW Australia experience a warm and wet season (Fig. 1a and b). Freshwater and terrigenous material reach the Sahul Shelf from the Victoria, Daly and Adelaide Rivers (NW Australia), and variations in riverine discharge depend on the strength of the austral summer monsoon (NW monsoon) (Fig. 2) [*Alongi et al.*, 2013]. However, most terrigenous material is not of Australian but of Indonesian origin, as about 30 rivers in the western part of New Guinea represent a significant source of sediments for the Arafura and Timor Sea due to the steep topography of New Guinea, promoting intense discharge (Fig. 2) [*Alongi et al.*, 2013]. In contrast, during the austral winter monsoon (SE monsoon), both the ITF and the Sahul Shelf currents flow to the southwest and are intensified, as the pressure gradient between

the Pacific and Indian Oceans is at its highest [*Cresswell et al.*, 1993; *Sprintall et al*., 2009; *Schiller et al*., 2011]. During the austral winter monsoon, the ITCZ retreats northward, and Indonesia and NW Australia experience a cool and dry season (Fig. 1c and d). Additionally, sea surface salinity increases toward the inner part of the Sahul Shelf owing to the excess in evaporation over precipitation leading to local dense water formation (Fig. 1d) [*Cresswell et al.*, 1993]. Evaporative dense water formation also occurs during austral winter on the inner NW Australian shelf (Fig. 1d) and denser water are transported at intermediate depth offshore, either via eddy transport or by transport in the boundary layers [*Brink and Sherman* 2006; *Brink et al*., 2007; *Shearman and Brink* 2010].

During periods of lowered sea level, the exposure of vast shelf areas in the western Pacific, such as the Sahul Shelf, the Arafura Shelf and Gulf of Carpentaria, drastically altered local circulation and sedimentation due to changes in the geometry of pathways connecting local seas as well as displacement of depositional basins (Fig. 2) [*Wang et al.*, 1999; *Reeves et al*., 2008]. Paleoclimate records of surface temperature and salinity indicated that the ITF varied considerably during the last glacial cycle due to sea level-driven alterations in the influx of cooler and fresher waters into the Indonesian seas and to variations in monsoon activity modulated by insolation changes [e.g.: *Lea et al*., 2000; *Visser et al.*, 2003; *Spooner et al.*, 2005; *Beaufort et al.*, 2010; *Linsley et al*., 2010]. In the Timor Sea, paired records of surface and upper thermocline temperature and salinity spanning the last glacial cycle indicated that the upper thermocline showed higher variability than the surface flow [e.g. *Xu et al.*, 2006, 2008; *Holbourn et al.*, 2011; *Ding et al.*, 2013]. These studies revealed cooling and freshening of the upper thermocline

during sea level highstands, which was interpreted as an intensification of the ITF thermocline flow. A weaker and more surface-dominated glacial ITF was also proposed by *Žuvela-Aloise* [2005], based on numerical circulation models. Only one recent study [*Rosenthal et al*., 2013] focused on temperature and salinity reconstructions of the deeper component of the ITF. This work, based on a suite of sediment cores retrieved from the Makassar Strait and Flores Sea, revealed a distinct warming of intermediate waters during the early Holocene maximum in Northern Hemisphere summer insolation [*Rosenthal et al*., 2013]. These authors suggested that warming of the ITF source water at higher latitudes controls intermediate water temperature variability in the Indonesian seas [*Rosenthal et al*., 2013]. However, this study does not allow assessment of longer-term glacial – interglacial variability and relations to changing climatic boundary conditions (e.g., ice volume, sea level, seaway geometry, interhemispheric thermal gradient).

3. Material and methods

3.1 Sampling strategy

During the Sonne-185 "VITAL" Cruise [*Kuhnt et al*., 2005], piston-core SO18471 (9° 21.987' S, 129° 58.983'E; 485 m water depth; 13.5 m length) was retrieved at the southern edge of the Timor Strait, close to the Sahul Shelf as part of a NE-SW transect across the Timor Sea (Fig. 1). The sediment consists of hemipelagic foraminiferal ooze and bioturbation is common throughout the record. A total of 134 sediment samples (1 cm thick sediment slices) were taken in 10 cm intervals between 0 and 1330 cm (0-133 ka), corresponding on average to 1 kyr time resolution. In the intervals between 0 and 120

cm and between 400 and 750 cm, additional samples were taken in 5 cm intervals to increase the temporal resolution.

3.2 Percentage of coarse material (>63 μm)

Sediment samples were oven-dried below 40 °C, weighed, disaggregated by soaking in water and wet sieved over a 63 μm screen. Residues were dried on a sheet of filter paper below 40 °C, then weighed and sieved into 63-150 μm, 150-250 μm, 250-315 μm, >315 μm fractions. The percentage of coarse material (>63 μm) was calculated as follows:

Residue dry weight/original dry weight*100.

3.3 Accelerator mass spectrometry ^{14}C dating

For accelerator mass spectrometry (AMS) ^{14}C dating, approximately 800 well preserved tests of *Globigerinoides ruber* were picked from the >250 μm fraction in six samples from core SO18471. *Globigerinoides sacculifer* tests were additionally picked in two samples due to the scarcity of *G. ruber* (Table 1). Conventional ^{14}C ages were determined at the Leibniz Laboratory for Radiometric Dating and Isotope Research (Leibniz Laboratory), University of Kiel, using standard methods described by *Nadeau et al.* [1997] and *Grootes et al*. [2004]. Conventional AMS ^{14}C ages were converted into calendar ages using the radiocarbon calibration program CALIB REV7.1.0 [*Stuiver and Reimer*, 1993] and the calibration data set IntCal13 [*Reimer et al.*, 2013]. A reservoir correction of 475 years was applied following *Southon et al*. [2002].

3.4 Stable isotope analysis

Between 15 and 30 tests of *Hoeglundina elegans* and *Uvigerina* spp. were selected for stable isotope and Mg/Ca analysis from the >250 µm size fraction and ~30 tests of *G. ruber* were picked from the size fraction 250-315 µm. Tests were checked under the microscope for cement encrustations and infillings before being broken into large fragments. After crushing, foraminiferal samples were split into Mg/Ca sub-samples (2/3 of the total sample) and $\delta^{18}O$ sub-samples (remaining 1/3) to obtain more homogeneous and representative material for measurement. The split samples for stable isotope analysis were cleaned in ethanol in an ultrasonic bath and dried at 40 °C. Stable isotopes were measured with a Finnigan MAT 253 mass spectrometer at the Leibniz Laboratory, University of Kiel. The instrument is coupled on-line to a Carbo-Kiel Device (Type IV) for automated CO_2 preparation from carbonate samples for isotopic analysis. On the basis of the performance of international and lab-internal standard carbonates, the precision is better than ±0.09‰. Results were calibrated using the NIST (National Institute of Standard and Technology, Gaithersburg, Maryland) carbonate isotope standard and NBS (National Bureau of Standard) 19 and in addition NBS 20, and are reported on the Vienna PeeDee Belemnite (VPDB) scale. Replicate measurements on twenty-five pairs of *H. elegans* indicate a mean reproducibility of ±0.09‰ for $\delta^{18}O$, 34 replicate samples of *Uvigerina* spp. a mean reproducibility of ±0.08‰ for $\delta^{18}O$; 62 replicate samples of *G. ruber* a mean reproducibility of ±0.10‰ for $\delta^{18}O$.

3.5 X-ray fluorescence core scanning

The archive half of core SO18471 was scanned for major element intensities in 1 cm resolution at the Institute of Geosciences, University of Kiel, using the second generation Avaatech X-ray fluorescence core scanner. The core was covered with a 4 μm-thin SPEXCerti Prep Ultralene1 foil to avoid contamination of the XRF measurement unit and desiccation of the sediment. Intensities of elements common in continental siliciclastic rocks (e.g. Fe, Ti, Al, Si, K) are used as qualitative proxies for terrigenous input, normalized against calcium derived from biogenic carbonate and reported as log ratios to reduce the risk of measurement artifacts from variable signal intensities and matrix effects [*Weltje and Tjallingii*, 2008; *Kuhnt et al.*, 2015]. The log ratio of Zr/Rb is used as a grain size proxy, as Zirconium tends to be associated with coarser particles than Rubidium [e.g.: *Calvert and Pedersen*, 2007]. Zirconium is one of the main components of heavy minerals, such as zircon, which is subject to sorting and preferential settling on the continental shelf [*Lourens et al.*, 2001; *Kuhnt et al*., 2015].

3.6 Carbonate content

Carbonate content was measured on dried and crushed bulk sediment samples by full reaction with 6 N HCl, using a "carbonate bomb" device [*Müller and Gastner*, 1971] at the Institute of Geosciences, University of Kiel. In intervals where prominent changes in the XRF-derived terrigenous input record occurred, carbonate content was measured with a resolution of approximately 50 cm. Standard error of the carbonate bomb device is ±1%.

3.7 Mg/Ca temperature estimates

Sea surface temperatures (SST) and bottom water temperatures (BWT) were estimated from Mg/Ca ratios of *G. ruber* and *H. elegans*, respectively. Samples were cleaned of the contaminant phases using the cleaning procedure with reductive step detailed in *Martin and Lea* [2002] and were analyzed with the ICP-OES (Inductively Coupled Plasma-Optical Emission Spectrometer) (Spectro Ciros SOP) with cooled cyclonic spraychamber and microconcentric nebulization (200 µl min^{-1}) at the Institute of Geosciences, University of Kiel. Intensity ratio calibration followed the method of *de Villiers et al.* [2002] and internal analytical precision was 0.1-0.2%. A dissolution-induced decrease of Mg/Ca, usually occurring in bottom waters with calcite-saturation states ($\Delta[CO_3^{2-}]_{calcite}$) below 21 µmol kg^{-1}, can be neglected, as core SO18471 has a modern bottom water $\Delta[CO_3^{2-}]_{calcite}$ of ~38 µmol kg^{-1}, well above the Mg/Ca lysocline [*Regenberg et al.*, 2014].

We converted *G. ruber* Mg/Ca ratios into temperatures using the calibration: Mg/Ca = 0.38±0.02 exp (0.09±0.003) SST from *Anand et al.* [2003]. For *H. elegans*, we used the equation: Mg/Ca = 0.31±0.06 exp (0.14±0.01) BWT from *Lo Giudice Cappelli et al.* [2015]. Errors in SST and BWT reconstructions were calculated by propagating the errors introduced by Mg/Ca measurements and the Mg/Ca temperature calibrations mentioned above, following the approach described in *Mohtadi et al.* [2014]. Potential effects of glacial - interglacial sea level changes on BWT are discussed in the Supplementary Material.

Replicate measurements on 27 pairs of *H. elegans* gave a reproducibility of ±0.19 mmol mol^{-1} (standard deviation), corresponding to a temperature difference of ±1.2 °C.

No duplicate measurements of *G. ruber* were performed. However according to *Xu et al*. [2006], who applied the same cleaning procedure and used the same analytical setup, sample reproducibility in *G. ruber* for a nearby core in the Timor Sea is ±0.7 °C, based on the calibration of *Anand et al.* [2003] for 24 replicate samples. Foraminiferal Fe/Ca, Al/Ca and Mn/Ca ratios were additionally used to monitor cleaning efficacy and no correlation with Mg/Ca ratios was found. However, one *G. ruber* and 9 *H. elegans* samples were not included in this study, as they showed high trace elements ratios indicative of contamination. Additionally, five *H. elegans* samples did not have enough material for measurement. From 1142 cm to the base of the core, the cleaning procedure was affected by the higher pyrite content of the samples and an additional 11 samples were rejected.

3.8 Sea water $\delta^{18}O$ ($\delta^{18}O_{sw}$) reconstructions

We calculated seawater $\delta^{18}O$ ($\delta^{18}O_{sw}$) from $\delta^{18}O$ of the foraminiferal calcite ($\delta^{18}O_{foram}$) and Mg/Ca-based temperature estimates for both surface and lower thermocline waters in core SO18471. We applied the equation: SST = (16.5 ± 0.2) – (4.80 ± 0.16) ($\delta^{18}O_{G.ruber}$ - $\delta^{18}O_{sw}$ + 0.27) from *Bemis et al.* [1998] to calculate $\delta^{18}O_{sw}$ in surface waters, and the equation: $\delta^{18}O_{sw}$ = 0.27 + $\delta^{18}O_{H.elegans}$+ (0.237 ± 0.003) BWT - (4.75 ± 0.04) from *Marchitto et al.* [2014] to calculate $\delta^{18}O_{sw}$ in bottom waters. In both cases, we corrected $\delta^{18}O_{sw}$ for ice volume using the sea level curve of *Waelbroeck et al.* [2002] adjusted to the chronology of core SO18471. Errors in $\delta^{18}O_{sw}$ reconstructions were calculated by propagating the errors introduced by $\delta^{18}O_{foram}$ measurements and the $\delta^{18}O$

temperature calibrations of *Bemis et al.* [1998] and *Marchitto et al.* [2014], following the approach described in *Mohtadi et al.* [2014].

4. Results

4.1 Chronology

The age model for the last 35 ka is based on six AMS ^{14}C dates in the upper 250 cm of the core (Table 1). Between 250 and 1242 cm, we correlated the *Uvigerina* spp., the *H. elegans* and the *G. ruber* δ^{18}O curves with the EDML-1 Antarctica ice core record (AICC2012) [*Veres et al*., 2013], using seven tie points (Table 1 and Fig. 3). The final age model was generated by linear interpolation between AMS ^{14}C ages and tie points (Fig. 3e). *Uvigerina* spp. and *H. elegans* δ^{18}O values recorded at the base of core SO18471 are between ~0.6 and 0.4‰ lower than during Marine Isotope Stage (MIS) 2, and between ~0.3 and 0.2‰ lower than during MIS 4, indicating that the base of the core is still within Termination II, well above the MIS 6 δ^{18}O maximum at 138 ka (Fig. 3). A marked glacial-interglacial contrast is evident in the sedimentation rate, which is ~6 cm kyr^{-1} during MIS 5 and ~3 cm kyr^{-1} during the Holocene and fluctuates between ~9 and ~17 cm kyr^{-1} from MIS 4 to MIS 2 (Fig. 3f).

4.2 Terrigenous discharge/ river runoff

We used log((Fe+Ti+Al+Si+K)/Ca) and carbonate content as proxies for terrigenous discharge/river runoff, where higher log((Fe+Ti+Al+Si+K)/Ca) ratios and lower carbonate content indicate dominance of terrigenous-derived sediments.

Fluctuations in both parameters generally follow glacial – interglacial cycles, with increased terrigenous input during periods of low sea level and closer proximity to the coast, and reduced terrigenous input during periods of high sea level and increased distance from the coast (Fig. 4d and e). However, during MIS 5e, when sea level was at its highest, terrigenous input was higher than during MIS 1 (Fig. 4d and e).

4.3 Grain size and heavy minerals

We used the percentage of coarse material (>63 μm) (Fig. 4c) and log(Zr/Rb) (Fig. 4b) as qualitative measures of sediment grain size. Both proxies follow the same glacial – interglacial trend, with higher values during sea level highstands and lower values during sea level lowstands (Fig. 4). As for the terrigenous proxy data, an exception to this trend is evident, however, during MIS 5e, when low values were recorded despite the highest sea level (Fig. 4).

4.4. Stable isotopes

Due to the scarcity of *H. elegans* and the occurrence of two different morphotypes in one interval of core SO18471 (Supplementary Fig. 2), we additionally measured *Uvigerina* spp. to obtain a higher resolution $\delta^{18}O$ record (Figs. 6a and b). *Hoeglundina elegans* $\delta^{18}O$ varies between 2.24 and 3.88‰, whereas *Uvigerina* spp. $\delta^{18}O$ ranges from 1.63 to 3.40‰ (Figs. 6a and b). We measured $\delta^{18}O$ in 103 paired-samples of *H. elegans* and *Uvigerina* spp. to calculate the $\delta^{18}O$ offset between the two species ($\Delta\delta^{18}O = \delta^{18}O_{H.elegans}-\delta^{18}O_{Uvigerina\ spp} = 0.62‰$, on average). The offset is quite consistent over the

entire core (standard deviation 0.17‰) and can be used to produce an intercalibrated benthic $\delta^{18}O$ curve by adding 0.62‰ to the $\delta^{18}O$ values of *Uvigerina* spp. (Supplementary Fig. 3).

The *Uvigerina* spp. and *H. elegans* $\delta^{18}O$ records generally show a well-defined glacial – interglacial variability (Figs. 6a and b). The lowest *Uvigerina* spp. $\delta^{18}O$ value (1.63‰) is detected during MIS 5e (~129 ka) and the highest (3.40‰) occurs during MIS 2 (~24 ka) (Fig. 6a). Similarly, the lowest *H. elegans* $\delta^{18}O$ value (2.24‰) is detected during MIS 5e (~125 ka) and the highest (3.87‰) occurs during MIS 2 (~26 ka) (Fig. 6b). The glacial - interglacial $\delta^{18}O$ contrast between MIS 2 and the Holocene is 1.3‰ for *H. elegans* and 1.4‰ for *Uvigerina* spp. Between MIS 5e and the base of the record (~133 ka) the difference is only 1.2‰ for *H. elegans* and 1.1‰ for *Uvigerina* spp., implying that the base of the core extends to Termination II and does not reach MIS 6 (Figs. 6a and b). Additionally, significant variability is evident during MIS 3 (Figs. 6a and b).

The *G. ruber* $\delta^{18}O$ record also displays a strong glacial – interglacial signal (Fig. 5a), with values oscillating between -2.90 and -1.10‰. During MIS 5, *G. ruber* $\delta^{18}O$ values varied between -2.90 and -1.96‰, increasing to a maximum of -1.30‰ during MIS 4. During MIS 3, $\delta^{18}O$ values fluctuated between -1.92 and -1.14‰, then decreased rapidly from -1.11 to -2.62‰ between 21.1 and 7.9 ka. The difference between glacial and interglacial *G. ruber* $\delta^{18}O$ is 1.63‰ between MIS 2 and the Holocene and 1.10‰ between MIS 5e and the base of the record (Fig. 5a).

4.5 Sea surface temperature

Mg/Ca ratios in *G. ruber* vary between 3.23 and 5.39 mmol mol^{-1}, corresponding to SSTs ranging from 23.8 to 29.5 °C, in comparison to a modern annual average SST of 28.4 °C (*World Ocean Atlas 2005* data [*Locarnini et al.,* 2006]) (Fig. 5b). During austral summer (January-March), modern SST is on average 29 °C, while during austral winter (July-September) it is 26.8 °C (Fig. 1a and c).

Mean SSTs were ~28 °C during MIS 5, close to the modern day average, with the warmest SSTs (~29 °C) recorded during MIS 5e. In contrast, during the globally cold period from MIS 4 to MIS 2, SSTs were on average 25.8 °C, about 2.6 °C lower than today. However, SSTs were ~1°C warmer during MIS 4 in comparison to MIS2. During Termination I, SST displays a steady rise, reaching 28°C in the Holocene, which is ~1 °C lower than during MIS 5e (Fig. 5b).

4.6 Bottom water temperature

Mg/Ca ratios in *H. elegans* vary between 0.73 and 2.01 mmol mol^{-1} corresponding to BWTs between 6.1 and 13.3 °C, in comparison to a modern annual average of 8.1 °C at 500 m (*World Ocean Atlas 2005* data [*Locarnini et al.,* 2006]) (Figs. 1e and 6c). Between 130 and 125 ka, BWTs were ~3 °C higher than today, fluctuating around 11 °C (Fig. 6c). In the late part of MIS 5e and through MIS 5, an overall cooling trend is detected: from 11.2 °C at 125.7 ka to 8.4 °C at 71.4 ka. The beginning of the cooling is marked by a sharp drop of ~3 °C in BWT between 125 and 115 ka (Fig. 6c). Relatively high BWTs (~9.5 °C) are recorded during the cold period from MIS 4 to MIS 2. The most conspicuous increase appears to occur during the early part of MIS 3 between ~56 and 52

ka, when BWT increased from 7.9 °C to 13.3 °C (Fig. 6c). However, as a thin-walled morphotype of *H. elegans* preferentially occurs (Supplementary Fig. 2) and the overall abundance of this species is low within this interval, it is difficult to assess whether these higher Mg/Ca ratios reflect an actual increase in BWT or are biased by the chemical composition of the thin-walled *H. elegans* morphotype. As we do not know whether these measurements are representative, we did not connect these higher values to the rest of the temperature record (Fig. 6c). However, *Corrège and De Deckker* [1997] recorded warm intermediate waters during early MIS 3 in the Coral Sea, suggesting that BWT may have increased off the northern coast of Australia during this period. During Termination I and throughout the Holocene, BWT decreased from 11 °C at 15 ka to 8.6 °C at 1.5 ka, with a sharp transient increase to 10 °C centered at 10.6 ka (Fig. 6c).

4.7 $\delta^{18}O_{sw}$ reconstructions

Surface and lower thermocline $\delta^{18}O_{sw}$ were calculated from $\delta^{18}O_{G.ruber}$ and $\delta^{18}O_{H.elegans}$ and corrected for temperature and ice volume effects. Surface $\delta^{18}O_{sw}$ ranges between -0.47 and 0.56‰ with generally higher values during MIS 5 (on average of ~0.14‰) and lower values between MIS 4 and MIS 2 (on average ~-0.08‰) (Fig. 5c). In contrast, lower thermocline $\delta^{18}O_{sw}$ values fluctuate between -0.30 and 1.41‰ with overall lower values during MIS 5 (on average ~0.37‰) and higher values between MIS 4 and MIS 2 (on average ~0.74‰).

5. Discussion

5.1 Sedimentation dynamics in the Timor Strait over the last 130 ka

During glacial periods, the most striking change in the geomorphology of Australasia was the exposure of vast shelf areas, such as the Sahul Shelf, the Arafura Shelf and the Gulf of Carpentaria [*Wang et al.*, 1999]. Marginal seas, such as the Timor and Arafura seas, were very sensitive to glacial sea level lowering, as changes in the proximity to exposed shelves affected local sedimentation and circulation [*Wang et al.*, 1999]. During sea level lowstands, core SO18471 was deeply influenced by the proximity of the exposed Sahul Shelf, resulting in generally higher terrigenous input (higher log(Fe+Ti+Al+Si+K/Ca) values) and lower carbonate content due to erosion of the emerged shelf during dry periods and increased discharge during humid periods, depending on the monsoon cycle (Figs. 4d and e). During sea level highstands, the location of core SO18471 was more distal from land and terrigenous input to the core location was more muted and dependent on the intensity of regional monsoonal rainfall and river runoff. Furthermore, the marked glacial – interglacial contrast in sedimentation rate in core SO18471 over the last ~130 ka (3-6 cm ky^{-1} during MIS 5 and the Holocene in contrast to 11-17 cm ky^{-1} between MIS 4 and 2) (Fig. 3f) supports a decrease in terrigenous input during sea level highstands.

An exception to this glacial – interglacial trend is evident during MIS 5e, when higher terrigenous input and sedimentation rate in comparison to the Holocene suggest that the regional monsoon signal overrides the sea level effect (Figs. 3f and 4d). At this time Northern Hemisphere summer insolation was high (Fig. 6e) causing melting of

northern ice sheets and consequently promoting slowdown in the Meridional Overturning Circulation, which in turn generated cold anomalies in the North Atlantic [*Broecker et al.*, 1985; *McManus et al.*, 1999; *Cheng et al.*, 2009]. This may have resulted in a southern displacement of the ITCZ [*Wang et al*., 2004; *Chiang et al.*, 2005; *Broccoli et al.*, 2006; *Mohtadi et al*., 2011; *Carolin et al*., 2013; *Huang et al*., 2015] and warming of the Southern Hemisphere and Antarctica [*Petit et al*., 1999; *Pépin et al.*, 2001]. Warmer Southern Hemisphere and Antarctica may have amplified local monsoon forcing [*Petit et al.*, 1999; *Pépin et al.*, 2001] by increasing heat and moisture supply to the atmosphere, eventually resulting in wet conditions and thus higher terrigenous input at the core location during MIS 5e (Fig. 4d). This is in agreement with a recent study proposing increased rainfall over southern Indonesia and northern Australia during Termination II [*Huang et al.*, 2015] and with the monsoon record from Lake Eyre correlating high-lake-level events with a more effective penetration of monsoon moisture into continental Australia [*Magee et al*., 2004; *Habeck-Fardy and Nanson*, 2014].

An alternative explanation is that the enhanced delivery of terrigenous material during MIS 5e was associated with increased tectonic activity in the hinterland, as several studies [e.g.: *Chappell and Veeh*, 1978; *Merritts et al.*, 1998; *Whitney and Hengesh*, 2015] reported uplift during Termination II and MIS 5e in eastern Indonesia and along the NW Australian coast. Although the reported rates of deformation were low, their contribution to the regional change in relative sea level is not negligible and might have influenced local sedimentation dynamics [*Whitney and Hengesh*, 2015].

5.2 Secular variations in ITF intensity

Both grain size proxies, the log(Zr/Rb) and percentage of coarse material (>63μm), show a strong glacial – interglacial trend, which mirrors the terrigenous input record (Fig. 4). Coarser material prevailed during sea level highstands (MIS 5 and 1), when core SO18471 was in a more distal location from land, whereas finer sediments dominated during sea level lowstands (MIS 4 and 2) (Figs. 4b, c and e). This unusual pattern likely reflects the effect of sediment winnowing by intensified bottom currents during sea level highstands, whereas at times of low sea level weaker bottom currents were unable to transport clays away (Figs. 4b, c and e). Given the location and relatively shallow water depth of core SO18471, these variations in bottom current activity are plausibly related to changes in ITF intensity.

An exception to this glacial – interglacial trend is evident during MIS 5e, when both grain size records exhibit low values, comparable with low sea level rather than high sea level values (Figs. 4b, c and e). A possible explanation is that the local monsoon signal overrides the sea level effect, as seen for the terrigenous input record (Fig. 4d). Intensification of the local monsoon may have promoted a marked increase in the riverine discharge of clay minerals (Fig. 4d) resulting in a decreased percentage of coarser terrigenous material (i.e.: aeolian dust) and lower log(Zr/Rb) at the location of core SO18471 (Figs. 4b and c).

Discrepancies between the two grain size records are also evident during MIS 5b and MIS 5a, when sharp increases were captured in the percentage of coarse material (Fig. 4c) in contrast to the more stable log(Zr/Rb) record (Fig. 4b). The coarse material is dominated by calcareous biogenic components, which are not reflected in the log (Zr/Rb)

record. Therefore, the increases in the percentage of coarse material during MIS 5b and MIS 5a may be partly due to variations in the accumulation of biogenic carbonate rather than to changes in winnowing by an intensified ITF (Figs. 4b and c). This is also supported by a substantial increase in carbonate content during MIS 5a (Fig. 4d).

5.3 Hydrological variability during the last glacial cycle

5.3.1 Long-term variability

Surface and lower thermocline temperature and $\delta^{18}O_{sw}$ records show a glacial – interglacial trend: the surface is generally warmer (on average by ~2 °C) and saltier during globally warm periods (MIS 5a-d and 1), whereas the lower thermocline is generally cooler (on average by ~1.4 °C) and fresher than during globally cold periods (from MIS 4 to MIS 2) (Figs. 5 and 6). This most likely reflects the intensification and expansion of a cool and fresh thermocline ITF during sea level highstands (Figs. 4b and c), resulting in generally cool and fresh bottom waters at the core location (Figs. 6c and d). In contrast, the thermocline shoaled between MIS 4 and 2, when bottom waters became warmer and saltier at the location of core SO18471 (Figs. 6c and d). However, early MIS 5e exhibits relatively warm lower thermocline temperatures (~11 °C) and no clear freshening signal in the benthic $\delta^{18}O_{sw}$ (Figs. 6c and d), indicating a more contracted thermocline ITF (Figs. 4b and c).

Sprintall et al. [2009] highlighted the importance of the contribution of warm and salty Indian Ocean waters, reaching the Banda Sea via the Ombai and Timor straits, to the formation of the modern outflow into the Indian Ocean. *Holbourn et al.* [2011] tracked

the evolution of water masses in the Timor Sea over the past 140 ka and found that during globally cold periods the deeper, cool and fresh, ITF component was reduced in the Timor Sea, where the influence of warm and salty Indian Ocean water became increasingly dominant. In core SO18471, we found a warmer and saltier lower thermocline flow (Fig. 6c and d) synchronous with periods of reduced ITF intensity (Figs. 4b and c), supporting advection of warmer and saltier Indian Ocean waters at the core location.

5.3.2 Summer monsoon intensification during MIS 3 and MIS 2?

Freshening of surface water at 56-50 ka and 28-23 ka during the early part of MIS 3 and MIS 2 (Fig. 5c) suggests transient intensifications of the austral summer monsoon. This was a period of globally cold SSTs with a significant reduction in the extension of the Indo Pacific Warm Pool (IPWP) and in the heat and vapor supply from the sea to the atmosphere [*De Deckker and Yokoyama*, 2009; *Wang et al.*, 1999]. During the LGM, SSTs were ~3 to 4 °C colder than during the Holocene on the Ontong Java Plateau [*Lea et al*., 2000], in the Makassar Strait [*Visser et al*., 2003], in the Timor Sea [*Xu et al*., 2008] and at the core location (Fig. 5b). However, speleothem records from Flores and NW Australia [*Lewis et al.*, 2011; *Ayliffe et al.*, 2013; *Denniston et al*., 2013] and marine sediment records from the Timor Sea and the western Banda Sea [*Muller et al*., 2008; *Kuhnt et al*., 2015] support a southern displacement of the ITCZ during the early part of MIS 2 that would account for freshening of surface waters at the location of core SO18471 (Fig. 5c) and relatively wet conditions in the southern tropics [*Reeves et al.*, 2013]. Increased precipitation might have resulted in more stratified waters, with a freshwater cap at the core location (Fig. 5c), and in alteration of the vertical structure of

the ITF (Figs. 6c and d). Additionally, monsoon records from continental Australia (Lake Eyre and Lake Mega-Frome) indicated that the last significant lacustrine event in Lake Eyre, and the establishment of connection between this basin and the adjacent Lake Mega Frome (coalescence of Lake Frome, Blanche, Callabonna and Gregory) occurred during the early part of MIS 3. These events have been related to the more effective penetration of austral summer monsoon moisture into Australia continental interior [*Magee et al*., 2004; *Cohen et al*., 2011; *Cohen et al*., 2012; *Habeck-Fardy and Nanson*, 2014].

An alternative view is that surface freshening during the early part of MIS 3 and MIS 2 in the Timor Strait may be related to regional hydrological changes. In the IPWP, *G. ruber* $\delta^{18}O_{sw}$ has been interpreted as a proxy for large-scale oceanic variations in vapor supply to the atmosphere and excess precipitation over evaporation [e.g.: *Oppo et al*., 2007; *Gibbons et al.*, 2014; *Fraser et al.*, 2014]. However, the comparison of core SO18471, retrieved in proximity of the Sahul Shelf, with two Timor Sea records from more distal locations (cores SO18460 and MD01-2378, Fig. 2) [*Holbourn et al.*, 2011] suggests that local forcings drive SST and salinity variability at location of core SO18471 (Supplementary Figs. 4a and b).

5.3.3 Influence of far-field high-latitude climate events

To explain the warming of intermediate water in the Makassar Strait and Flores Sea during the early Holocene maximum in Northern Hemisphere summer insolation (~10 ka), *Rosenthal et al*. [2013] hypothesized that warming in the ITF source waters at higher latitudes is transferred at intermediate depth in the tropics. Thermocline warming at ~10 ka is also recorded in upper and lower thermocline records from the Timor Sea (Fig. 6c and Supplementary Fig. 4c). Warming of the upper and lower thermocline during

the early part of MIS 5e (Fig. 6c and Supplementary Fig. 4c) also coincides with the highest Northern Hemisphere summer insolation of the past 140 kyr (Fig. 6e). However, BWTs are higher during early MIS 5e (~11 °C) than the early Holocene (~10 °C) (Fig. 6c), most likely due to the higher Northern Hemisphere summer insolation during MIS 5e (Fig. 6e). Additionally, a temporal shutdown in the formation of Antarctic bottom water between 128 and 125 ka [*Hayes et al.,* 2014] may have contributed to warming of the lower thermocline in core SO18471 during MIS 5e and to the thermal contrast between the early MIS 5e and early Holocene (Fig. 6c).

6. Conclusion

Our records from sediment core SO18471, retrieved at the southern edge of the Timor Strait, close to the Sahul Shelf, provide new insights into local hydrological changes related to ITF variations, changes in the local monsoon system and shelf dynamics during the last 130 ka. Our results indicate that sediment winnowing and terrigenous discharge were largely controlled by glacial – interglacial sea level change and proximity to the coasts, with reduced discharge and strong bottom currents (ITF) during sea level highstands. However, increased terrigenous input together with weakening and warming of the ITF lower thermocline flow suggest intensification of the local wet monsoon during MIS 5e. The warmer and saltier thermocline between MIS 4 and MIS 2 indicates weakening and contraction of the cool and fresh thermocline ITF and advection of warm and salty Indian Ocean waters into the Timor Strait. High Northern Hemisphere summer insolation during the early MIS 5e and early Holocene additionally appears to have influenced thermocline temperature in the Timor Strait through warming of ITF source

waters at higher latitudes.

Acknowledgements

We are grateful to Dieter Garbe-Schönberg for ICP-OES measurements and Nils Andersen for stable isotopes analyses. We thank Yiming Wang for stimulating discussions and constructive suggestions. We also gratefully acknowledge the crew of the R/V *Sonne* for all their efforts during the SO-185 VITAL cruise. We thank Jessica Reeves and one anonymous reviewer for constructive reviews that helped us to improve the manuscript. Funding for this research was provided by the Marie Curie Action Plan, Seventh Framework Program (Grant n° 237922) and BMBF Grant 03G0185A (VITAL). Data presented in this paper are archived and available at www.pangaea.de.

Figure captions

Fig. 1. Monsoon-induced seasonal variations in temperature, salinity and wind trajectory in the tropical Indo-Pacific Ocean plotted with Ocean Data View [*Schlitzer*, 2013]. **a)** and **b)** Austral summer (January-March) seasonal SST and salinity variations. **c)** and **d)** Austral winter (July-September) seasonal SST and salinity variations. **e)** and **f)** Mean annual temperature and salinity at 400 m. Temperature and salinity data are from the World Ocean Atlas 2005 [*Locarnini et al*., 2006]. Superimposed are winds trajectories (arrows) in February (**a** and **b**) and August (**c** and **d**). Wind data are monthly averages for February and August 2005 from NCEP Reanalysis Dataset (http://www.esrl.noaa.gov/psd/). Black circle indicates location of core SO18471.

Fig. 2. Local map showing position of core SO18471 (this study) and cores SO18460 and MD01-2378 [*Holbourn et al*., 2011] and locations referred to in this study. Black contour lines show differences in topography and bathymetry between present day and LGM, when sea level was ~120 m lower. Basemap was generated with GeoMapApp (http://www.geomapapp.org) using the Global Multi-Resolution Topography synthesis database [*Ryan et al*., 2009].

Fig. 3. a) EDML-1 ice core $\delta^{18}O$ curve [*Veres et al*., 2013]. **b)** Core SO18471 *G. ruber* $\delta^{18}O$ record. c) Core SO18471 *H. elegans* $\delta^{18}O$ curve **d)** Core SO18471 *Uvigerina* spp. $\delta^{18}O$ record. **e)** Linear interpolation between AMS ^{14}C dates (red crosses) and $\delta^{18}O$

events used as tie points (green crosses). **d)** Changes in sedimentation rate over the last 133 ka.

Fig. 4. a) *G. ruber* $\delta^{18}O$ record in core SO18471. **b)** XRF-derived grain size record in core SO18471. **c)** Percentage of coarse material >63μm in core SO184741. **d)** XRF-derived terrigenous input record (light blue curve); red crosses indicate measured carbonate content. **e)** Sea level curve from *Waelbroeck et al.* [2002] adjusted to chronology of core SO18471; dashed line at -53 m indicates depth of Arafura Sill. Gray shadings mark glacial periods MIS 6, 4 and 2; dashed black lines mark onset of MIS 5 sub-stages.

Fig. 5. a) *G. ruber* $\delta^{18}O$ record in core SO184741. **b)** *G. ruber* Mg/Ca-derived sea surface temperature in core SO18471 (black curve); dashed line indicates modern sea surface temperature [*Locarnini et al*., 2006]. **c)** *G. ruber* $\delta^{18}O_{sw}$ record. Gray shadings mark glacial periods MIS 6, 4 and 2; dashed black lines mark onset of MIS 5 sub-stages.

Fig. 6. a) *Uvigerina* spp. $\delta^{18}O$ record in core SO18471. **b)** *H. elegans* $\delta^{18}O$ record in core SO184741. **c)** *H. elegans* Mg/Ca-derived bottom water temperature; dashed line indicates modern temperature at 500 m [*Locarnini et al*., 2006]. **d)** Benthic $\delta^{18}O_{sw}$ record in core SO18471. **e)** Summer solstice insolation at 65°N (black line) and 20°S (red line) [*Laskar et al.*, 2004]. Gray shadings mark glacial periods MIS 6, 4 and 2; dashed black lines mark onset of MIS 5 sub-stages.

References

Alongi, D. M., M. da Silva, R. J. Wasson, and S. Wirasantosa (2013), Sediment discharge and export of fluvial carbon and nutrients into the Arafura and Timor Seas: a regional synthesis, *Marine Geology*, *343*, 146-158, doi: 10.1016/j.margeo.2013.07.004.

Anand, P., H. Elderfield, and M.H. Conte (2003), Calibration of Mg/Ca thermometry in planktonic foraminifera from sediment trap time series, *Paleoceanography*, *18*(2), 1050, doi: 10.1029/2002PA000846.

Ayliffe, L. K., M. K. Gagan, J. Zhao, R. N. Drysdale, J. C. Hellstrom, W. S. Hantoro, M. L. Griffiths, H. Scott-Gagan, E. St Pierre, J. A. Cowley, and B. W. Suwargadi (2013), Rapid interhemispheric climate links via the Australasian monsoon during the last deglaciation, *Nature communications*, 4, 2908, doi: 10.1038/ncomms3908.

Beaufort, L., S. van der Kaars, F. C. Bassinot, and V. Moron (2010), Past dynamics of the Australian monsoon: precession, phase and links to the global monsoon concept, *Climate of the Past*, *6*, 695-706, doi: 10.5194/cp-6-695-2010.

Bemis, B. E., H. J. Spero, J. Bijma, and D. W. Lea (1998), Reevaluation of the oxygen isotopic composition of planktonic foraminifera: Experimental results and revised paleotemperature equations, *Paleoceanography*, *13*(2), 150-160, doi: 10.1029/98PA00070.

Brink, K. H., and R. K. Shearman (2006), Bottom boundary layer flow and salt injection from the continental shelf to slope, *Geophysical Research Letters*, *33*, L13608, doi: 10.1029/2006GL026311.

Brink, K. H., F. Bahr, and R. K. Shearman (2007), Alongshore currents and mesoscale variability near the shelf edge off northwestern Australia, *Journal of Geophysical Research, 112*, C05013, doi: 10.1029/2006JC003725.

Broccoli, A.J., K.A. Dahl, and R.J. Stouffer (2006), Response of the ITCZ to Northern Hemisphere cooling, *Geophysical Research Letters*, 33, L01702, doi: 10.1029/2005GL024546.

Broecker, W.S., D.M. Peteet, and D. Rind (1985), Does the ocean-atmosphere system have moree than one stable mode of operation?, *Nature*, 315, 21-26.

Calvert, E., and T. Pedersen (2007), Elemental proxies for palaeoclimatic and palaeoceanographic variability in marine sediments: interpretation and application, C. Hillaire-Marcel, A.D. Vernal (Eds.), *Proxies in Late Cenozoic Paleoceanography*, Elsevier, Amsterdam, pp. 567–644, doi: 10.1016/S1572-5480(07)01019-6.

Carolin, S. A., K. M. Cobb, J. F. Adkins, B. Clark, J. L. Conroy, S. Lejau, J. Malang, and A. Tuen (2013), Varied response of western Pacific hydrology to climate forcings over the last glacial period, *Science*, 340, 1564-1567, doi: 10.1026/science.1233797.

Chappell, J., and Veeh H. H. (1978), Late Quaternary tectonic movements and sea-level changes at Timor and Atauro Island, *Geological Society of America Bulletin*, 89, 356-368.

Cheng, H., L. Edwards, W. S. Broecker, G. H. Denton, X. Kong, Y. Wang, R. Zhang, and X. Wang (2009), Ice age terminations, *Science, 326*, 5950, 248-252, doi: 10.1126/science.1177840

Chiang, J. C. H., and C. M. Bitz (2005), Influence of high latitude ice cover on the marine Intertropical Convergence Zone, *Climate Dynamics*, 25, 5, 477-496, doi: 10.1007/s00382-005-0040-5.

Cohen, T. J., Nanson G. C., Jansen J. D., Jones B. G., Jacobs Z., Treble P., Price D. M., May J-H., Smith A. M., Ayliffe L. K., and Hellstrom J. C. (2011), Continental aridification and the vanishing of Australia's megalakes, |*Geology*, 39, 167-170, doi: 10.1130/G31518.1.

Cohen, T. J., Nanson G. C., Jansen J. D., Jones B. G., Jacobs Z., Larsen J. R., May J-H., Treble P., Price D. M., and Smith A. M. (2012), Late Quaternary mega-lakes fed by the northern and southern river system of central Australia: varying moisture sources and increased continental aridity, *Palaeogeography, Palaeoclimatology, Palaeoecology*, 356-357, 89-108, doi: 10.1016/j.palaeo.2011.06.023.

Corrège, T., and P. De Deckker (1997), Fauna1 and geochemical evidence for changes in intermediate water temperature and salinity in the western Coral Sea (northeast Australia) during the Late Quaternary, *Palaeogeography, Palaeoclimatology, Palaeoecology, 313*, 183-205.

Cresswell, G., A. Frische, J. Peterson, and D. Quadfasel (1993), Circulation in the Timor Sea, *Journal of Geophysical Research*, *98*(C8), 14379-14389, doi: 10.1029/93JC00317.

De Deckker, P., and Y. Yokoyama (2009), Micropaleontological evidence for Late Quaternary sea-level changes in Bonaparte Gulf, Australia, *Global and Planetary Change*, 66, 85-22, doi:10.1016/j.gloplacha.2008.03.012.

Denniston, R. F., K-H. Wyrwoll, Y. Asmerom, V. J. Polyak, W. F. Humphreys, J. Cugley, D. Woods, Z. LaPointe, J. Peota, and E. Greaves (2013), North Atlantic forcing of millennial-scale Indo-Australian monsoon dynamics during the Last Glacial period, *Quaternary Science Reviews*, 72, 159-168, doi: 10.1016/j.quascirev.2013.04.012.

de Villiers, S., M. Greaves, and H. Elderfield (2002), An intensity ratio calibration method for accurate determination of Mg/Ca and Sr/Ca of marine carbonates by ICP-AES, *Geochemistry, Geophysics, Geosystems*, *3*(1), 1001, doi: 10.1029/2001GC000169.

Ding, X., F. Bassinot, F. Guichard, and N. Q. Fang (2013), Indonesian Throughflow and monsoon activity records in the Timor Sea since the last glacial maximum, *Marine*

Micropaleontology, *101*, 115-126, doi: 10.1016/j.marmicro.2013.02.003.

Egbert, G. D., R. D. Ray (2001), Estimates of M_2 tidal energy dissipation from TOPEX/Poseidon altimeter data, *Journal of Geophysical Research*, 106(C10), 22475-22502, doi: 10.1029/2000JC000699.

Ffield, A. L., and A. L. Gordon (1992), Vertical Mixing in the Indonesian Thermocline, *Journal of Physical Oceanography*, *22*(2), 184-195.

Fraser, N., W. Kuhnt, A. Holbourn, T. Bolliet, N. Andersen, T. Blanz, and L. Beaufort (2014), Precipitation variability within the West Pacific Warm Pool over the past 120 ka: evidence from the Davao Gulf, southern Philippines, *Paleoceanography*, 29, doi: 10.1002/2013PA002599.

Gibbons, F. T., D. W. Oppo, M. Mothadi, Y. Rosenthal, J. Cheng, Z. Liu, B. K. Linsley (2014), Deglacial $\delta^{18}O$ and hydrological variability in the tropical Pacific and Indian Ocean, *Earth and Planetary Science Letters*, 387, 240-251, http://dx.doi.org/10.1016/j.epsl.2013.11.032.

Gordon, A. L., and R. A. Fine (1996), Pathway of water between the Pacific and Indian oceans in the Indonesian seas, *Nature*, *379*, 146-149, doi: 10.1038/379146a0.

Gordon, A. L., and R. D. Susanto (2001), Banda Sea surface-layer divergence, *Ocean*

Dynamics, 52, 2-10, doi: 10.1007/s10236-001-8172-6.

Gordon, A. L. (2005), Oceanography of the Indonesian seas and their throughflow, *Oceanography*, *18*(4), 14-27, http://dx.doi.org/10.5670/oceanog.2005.01.

Grootes, P.M., M.-J. Nadeau, A. Rieck (2004), ^{14}C-AMS at the Leibniz-Labor: radiometric dating and isotope research, *Nuclear Instruments and Methods in Physics Research B, 223-224*, 55-61.

Hautala, S.L., J.L. Reid, and N. Bray (1996), The distribution and mixing of Pacific water masses in the Indonesian Seas, *Journal of Geophysical Research*, 101,C5, 12375-12389, doi: 10.1029/96JC00037.

Habeck-Fardy, A., and G. C. Nanson (2014), Environmental character and history of the Lake Eyre Basin, one seventh of the Australian continent, *Earth-Science Reviews*, 132, 39-66, http://dx.doi.org/10.1016/j.earscirev.2014.02.003.

Hayes, C. T., A. Martínez-García, A. P. Hasenfratz, S. L. Jaccard, D. A. Hodell; D. M. Sigman, G. H. Hang, R. F. Anderson (2014), A stagnation event in the deep South Atlantic during the last interglacial period, *Science, 346*, 1514, doi: 10.1126/science.1256620.

Holbourn, A., W. Kuhnt, and J. Xu (2011), Indonesian Throughflow variability during

the last 130 ka: the Timor Sea outflow, The SE Asian gateway: history and tectonics of Australia-Asia collision, Geological Society, London, Special Publications, *355*, 283-303, doi: 10.1144/SP355.14.

Huang, E., J. Tian, and J. Liu (2015), Dynamics of the Australian-Indonesian monsoon across Termination II: implications of molecular biomarker reconstructions from the Timor Sea, *Palaeogeography, Palaeoclimatology, Palaeoecology*, 423, 32-43, doi: 10.1016/j.palaeo.2015.01.027.

Koch-Larrouy, A., M. Lengaigne, P. Terray, G. Madec, and S. Masson (2010), Tidal mixing in the Indonesian Seas and its effect on the tropical climate system, *Climate Dynamics, 34*, 891-904, doi: 10.1007/s00382-009-0642-4.

Kuhnt, W., et al. (2005), Cruise report SONNE-185 "Variability of the Indonesian Throughflow and Australasian climate history of the last 150000 years (VITAL)", report, Institut für Geowissenschaften, Christian-Albrechts-Universität zu Kiel, Kiel, Germany.

Kuhnt, W., A. Holbourn, J. Xu, B. Opdyke, P. De Deckker, U. Röhl, and M. Mudelsee (2015), Southern Hemisphere control on Australian monsoon variability during the late deglaciation and Holocene, Nature Communications, *6*, 5916, doi: 10.1038/ncomms6916.

Laskar, J., P. Robutel, F. Joutel, M. Gastineau, A C. M. Correeia, and B. Levrard (2004), A long-term numerical solution for the insolation quantities of the Earth, *Astronomy and*

Astrophysics, 428, 261-285, doi: 10.1051/0004-6361:20041335.

Lea, D. W., D. K. Pak, and H. J. Spero (2000), Climate Impact of Late Quaternary equatorial Pacific sea surface temperature variations, *Science, 289*, 1719, doi: 10.1126/science.289.5485.1719.

Lewis, S.C., M.K. Gagan, L.K. Ayliffe, J-X. Zhao, W.S. Hantoro, P.C. Treble, J.C. Hellstrom, A.N. LeGrande, M. Kelley, G.A. Schmidt, and B.W. Suwargadi (2011), High-resolution stalagmite reconstructions of Australian-Indonesian monsoon rainfall variability during Heinrich stadial 3 and Greenland interstadial 4, *Earth and Planetary Science Letters*, 303, 133-142, doi: 10.1016/j.epsl.2010.12.048.

Linsley, B.K., Y. Rosenthal, and D.W. Oppo (2010), Holocene evolution of the Indonesian throughflow and the western Pacific warm pool, *Nature Geoscience, 3*, 578-583, doi: 10.1038/NGEO920.

Locarnini, R. A., A. V. Mishonov, J. I. Antonov, T. P. Boyer, and H. E. Garcia (2006), World Ocean Atlas 2005, Volume 1: temperature. *In*: Levitus S. (ED.) *NOAA Atlas NESDIS61*. U.S. Government Printing Office, Washington, DC, 182.

Lo Giudice Cappelli, E., M. Regenberg, A. Holbourn, W. Kuhnt, D. Garbe-Schönberg, and N. Andersen (2015), Refining *C. wuellerstorfi* and *H. elegans* Mg/Ca temperature calibrations, *Marine Micropaleontology*, 121, 70-84, doi:

10.1016/j.marmicro.2015.10.001.

Lourens, L. J., R. Wehausen, H. J. Brumsack (2001), Geological constraints on tidal dissipation and dynamical ellipticity of the Earth over the past three million years, *Nature, 409*, 1029–1033, doi:10.1038/35059062.

Magee, J. W., N. A. Spooner, and D. Questiaux (2004), Continuous 150 k.y. monsoon record from Lake Eyre, Australia: insolation-forcing implications and unexpected Holocene failure, *Geology*, 32, 885-888, doi: 10.1130/G20672.1.

Marchitto, T.M., W.B. Curry, J. Lynch-Stieglitz, S.P. Bryan, K.M. Cobb, and D.C. Lund (2014), Improved oxygen isotope temperature calibrations for cosmopolitan benthic foraminifera, *Geochimica et Cosmochimica Acta, 130*, 1-11, doi: 10.1016/j.gca.2013.12.034.

Martin, P.A., and D. Lea (2002), A simple evaluation of cleaning procedures on fossil benthic foraminiferal Mg/Ca, *Geochemistry, Geophysics, Geosystems*, *3*(10), 8401, doi: 10.1029/2001GC000280.

McManus, J.F., D.W. Oppo, and J.L. Cullen (1999), A 0.5-million-year record of millennial-scale climate variability in the North Atlantic, *Science*, 283, 5404, 971-975, doi: 10.1126/science.283.5404.971.

Merritts, D., R. Eby, R. Harris, R. L. Edwards, and H. Chang (1998), Variable rates of Late Quaternary surface uplift along the Banda Arc-Australian plate collision zone, eastern Indonesia. *In*: Stewart, I.S., and C. Vita-Finzi (eds) *Coastal Tectonics*. Geological Society, London, Special Publications, 146, 213-224.

Mohtadi, M., D. W. Oppo, S. Steinke, J-B W. Stuut, R. De Pol-Holz, D. Hebbeln, and A. Lückge (2011), Glacial to Holocene swings of the Australian-Indonesian monsoon, *Nature Geoscience*, 4, 540-544, doi: 10.1038/NGEO1209.

Mohtadi, M., M. Prange, D. W. Oppo, R. De Pol-Holz, U. Merkel, X. Zhang, S. Steinke, and A. Lückge (2014), North Atlantic forcing of tropical Indian Ocean climate, *Nature, 509*, 76-80, doi: 10.1038/nature13196.

Moore, T. S., J. Marra, and A. Alkatari (2003), Response of the Banda Sea to the southeast monsoon, *Inter-Research Marine Ecology Progress Series*, 261, 41-49, doi: 10.3354/meps261041.

Müller, G., and M. Gastner (1971), The "Karbonat-Bombe", a simple device for the determination of carbonate content in sediments, soils, and other materials, *Neues Jahrbuch für Mineralogie – Monatshefte, 10*, 466-469.

Muller, J., M. Kylander, R. A. J. Wüst, D. Weiss, A. Martinez-Cortizas, A. N. LeGrande, T. Jennerjahn, H. Behling, W. T. Anderson, and G. Jacobson (2008), Possible evidence

for wet Heinrich phases in tropical NE Australia: the Lynch's Crater deposit, *Quaternary Science Reviews*, 27, 468-475, doi:10.1016/j.quascirev.2007.11.006.

Nadeau, M.-J., M. Schleicher, P.M. Grootes, H. Erlenkeuser, A. Gottdang, D.J.W. Mous, J.M. Sarnthein, and H. Willkomm (1997), The Leibniz-Labor AMS facility at the Christian-Albrechts University, Kiel, Germany, *Nuclear Instruments and Methods in Physics Research B, 123*, 22-30.

Oppo, D. W., G.A. Schmidt, and A.N. LeGrande (2007), Seawater isotope constrains on tropical hydrology during the Holocene, *Geophysical Research Letters*, 34, L13701, doi: 10.1029/2007GL030017.

Oppo, D.W., and Y. Rosenthal (2010), The Great Indo-Pacific Communicator, *Science*, *328*, 1492-1494, doi: 10.1126/science.1187273.

Pépin, L., D. Raynaud, J-M. Barnola, and M. F. Loutre (2001), Hemispheric roles of climate forcings during glacial-interglacial transitions as deduced from the Vostock record and LLN-sD model experiments, *Journal of Geophysical Research*, 106(23), 31885-31892, doi: 10.1029/2001JD900117.

Petit, J. R., J. Jouzel, D. Raynaud, N. I., Barkov, J.-M. Barnola, I. Basile, M. Bender, J. Chappellaz, M. Davis, G. Delaygue, M. Delmotte, V. M. Kotlyakov, M. Legrand, V. Y. Lipenkov, C. Lorius, L. Pépin, C. Ritz, E. Saltzman, and M. Stievenard (1999), Climate

and atmospheric history of the past 420,000 years from the Vostock ice core, Antarctica, *Nature, 399,* 429-436, doi:10.1038/20859.

Ray, R. D., G. D. Egbert, and S. Y. Erofeeva (2005), A brief overview of tides in the Indonesian seas, *Oceanography*, *18*(4), 74-79,http://dx.doi.org/10.5670/oceanog.2005.07.

Reeves, J. M., A. R. Chivas, A. García, S. Holt, M. J. J. Couapel, B. G. Jones, D. I. Cendón, and D. Fink (2008), The sedimentary record of palaeoenvironments and sea-level change in the Gulf of Carpentaria, Australia, through the last glacial cycle, *Quaternary International, 183,* 3-22, doi: 10.1016/j.quaint.2007.11.019.

Reeves, J.M., H.C. Bostock, L.K. Ayliffe et al. (2013), Palaeoenvironmental change in tropical Australasia over the last 30,000 years – a synthesis by the OZ-INTIMATE group, *Quaternary Science Reviews*, 74, 97-114, doi: 10.1016/j.quascirev.2012.11.027.

Regenberg M., A. Regenberg, D. Garbe-Schönberg, and D. W. Lea (2014), Global dissolution effects on planktonic foraminiferal Mg/Ca ratios controlled by the calcite-saturation state of bottom waters, *Paleoceanography*, 29, 127-142, doi: 10.1002/2013PA002429.

Reimer, P. J., et al. (2013), IntCal13 and Marine13 radiocarbon age calibration curves 0-50,000 years cal BP, *Radiocarbon*, 55, 1869-1887, doi: 10.2458/azu_js_rc.55.16947.

Rosenthal, Y., B. K. Linsley, D. W. Oppo (2013), Pacific ocean heat content during the past 10,000 years, *Science, 342*, 617, doi: 10.1126/science.1240837.

Ryan, W. B. F., et al. (2009), Global Multi-Resolution Topography synthesis, *Geochemistry Geophysics Geosystems, 10*, Q03014, doi: 10.1029/2008GC002332.

Shearman, R. K., and K. H. Brink (2010), Evaporative dense water formation and cross-shelf exchange over the northwest Australian inner shelf, *Journal of Geophysical Research, 115*, C06027, doi: 10.1029/2009JC005931.

Schiller, A. (2011), Ocean Circulation on the North Australian Shelf, *Continental Shelf Research, 31*, 1087-1095, doi: 10.1016/j.csr.2011.03.013.

Schlitzer, R., Ocean Data View, http://odv.awi.de, 2013.

Southon, J., M. Kashgarin, M. Fontugne, B. Metivier, and W. W-S. Yim (2002), Marine reservoir corrections for the Indian Ocean and Southeast Asia, *Radiocarbon*, 44, 167-180.

Spooner, M. I., T. T. Barrows, P. De Deckker, and M. Paterne (2005), Paleoceanography of the Banda Sea, and Late Pleistocene initiation of the Northwest Monsoon, *Global and Planetary Change*, *49*, 28-46, doi: 10.1016/j.gloplacha.2005.05.002.

Sprintall, J., S. E. Wijffels, R. Molcard, and I. Jaya (2009), Direct estimates of the

Indonesian Throughflow entering the Indian Ocean: 2004-2006, *Journal of Geophysical Research*, *114*, C07001, doi: 10.1029/2008JC005257.

Stuiver, M., and P. J. Reimer (1993), Extended 14C database and revised CALIB radiocarbon calibration program, *Radiocarbon*, 35, 215-230.

Talley, L. D., and J. Sprintall (2005), Deep expression of the Indonesian Throughflow: Indonesian Intermediate Water in the South Equatorial Current, *Journal of Geophysical Research*, *110*, C10009, doi: 10.1029/2004JC002826.

Veres, D., et al. (2013), The Antarctic ice core chronology (AICC2012): an optimized multi-parameter and multi-site dating approach for the last 120 thousand years, *Climate of the Past*, 9, 1733-1748, doi: 10.5194/cp-9-1733-2013.

Visser, K., R. Thunell, and L. Stott (2003), Magnitude and timing of temperature change in the Indo-Pacific warm pool during deglaciation, *Nature*, 421, 152-155, doi:10.1038/nature01297.

Waelbroeck, C., L. Labeyrie, E. Michel, J. C. Duplessy, J. F. McManus, K. Lambeck, E. Balbon, and M. Labracherie (2002), Sea-level and deep water temperature changes derived from benthic foraminifera isotopic record, *Quaternary Science Reviews*, *21*, 295-305, http://dx.doi.org/10.1016/S0277-3791(01)00101-9.

Wang, P. (1999), Response of Western Pacific marginal seas to glacial cycles: paleoceanographic and sedimentological features, *Marine Geology, 156*, 5-39.

Wang, X., A. S. Auler, R. L. Edwards, H. Cheng, P. S. Cristalli, P. L. Smart, D. A. Richards, and C-C Shen (2004), Wet periods in northeastern Brazil over the past 210 kyr linked to distant climate anomalies, *Nature*, 432, doi:10.1038/nature03067.

Weltje, G. J., and R. Tjallingii (2008), Calibration of XRF core scanners for quantitative geochemical logging of sediment cores: theory and application, *Earth and Planetary Science Letters, 274*(3), 423-438, doi: 10.1016/j.epsl.2008.07.054.

Whitney, B. B., and J. V. Hengesh (2015), Geomorphological evidence for late Quaternary tectonic deformation of the Cape Region, coastal west central Australia, Geomorphology, 241, 160-174, http://dx.doi.org/10.1016/j.geomorph.2015.04.010

Wijffels, S. E., G. Meyers, J. S. Godfrey (2008), A 20-Yr Average of the Indonesian Throughflow: Regional Currents and the Interbasin Exchange, *Journal of Physical Oceanography*, 38, 1965-1978, doi: 10.1175/2008JPO3987.1.

Xu, J., W. Kuhnt, A. Holbourn, N. Andersen, and G. Bartoli (2006), Changes in the vertical profile of the Indonesian Throughflow during Termination II: evidence from the Timor Sea, *Paleoceanography*, *21*, PA4202, doi: 10.1029/2006PA001278.

Xu, J., A. Holbourn, W. Kuhnt, Z. Jian, and H. Kawamura (2008), Changes in the thermocline structure of the Indonesian outflow during Terminations I and II, *Earth and Planetary Science Letters*, *273*, 152-162, doi: 10.1016/j.epsl.2008.06.029.

Žuvela-Aloise, M. (2005), Modelling of the Indonesian Throughflow on glacial-interglacial timescales, Ph.D thesis, Mathematisch-Naturwissenschaftliche Fakultät, Christian-Albrechts-Universität zu Kiel, Germany.

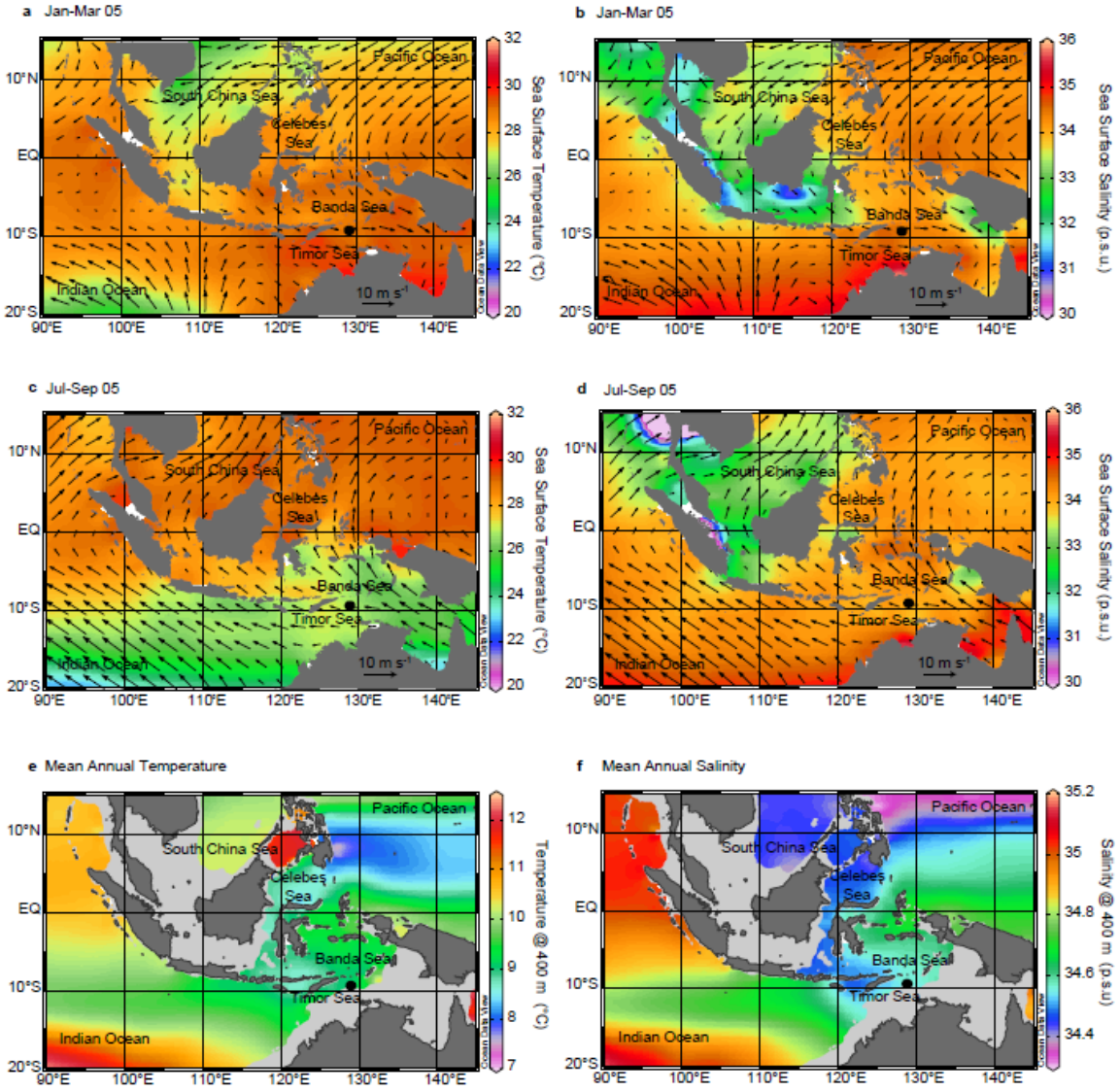

Fig. 1

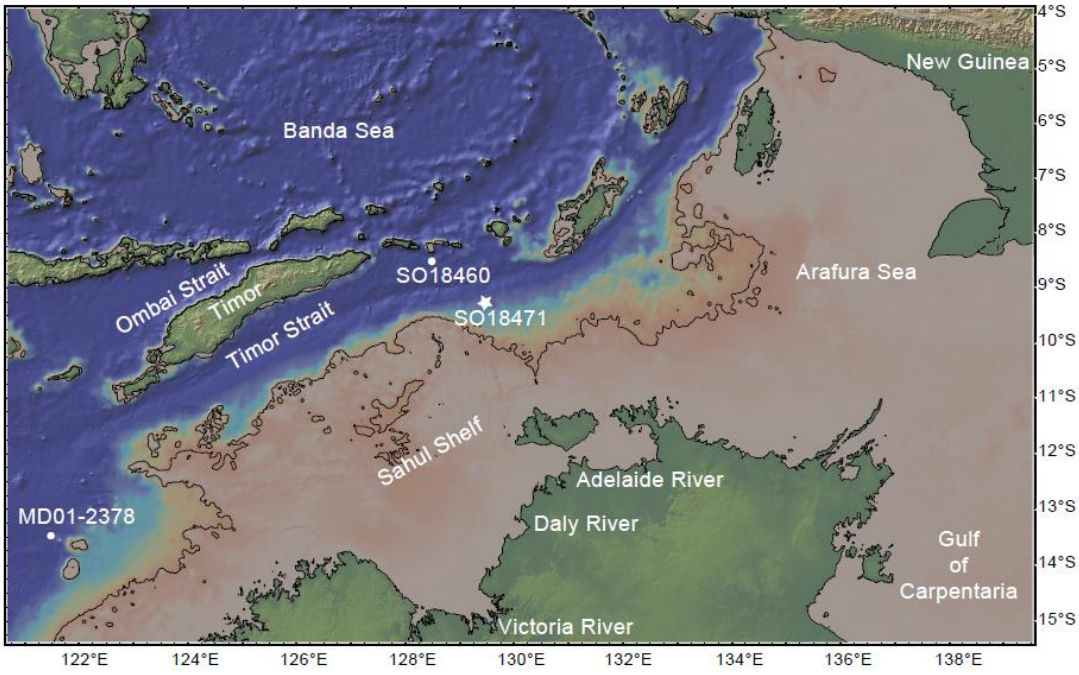

Fig. 2

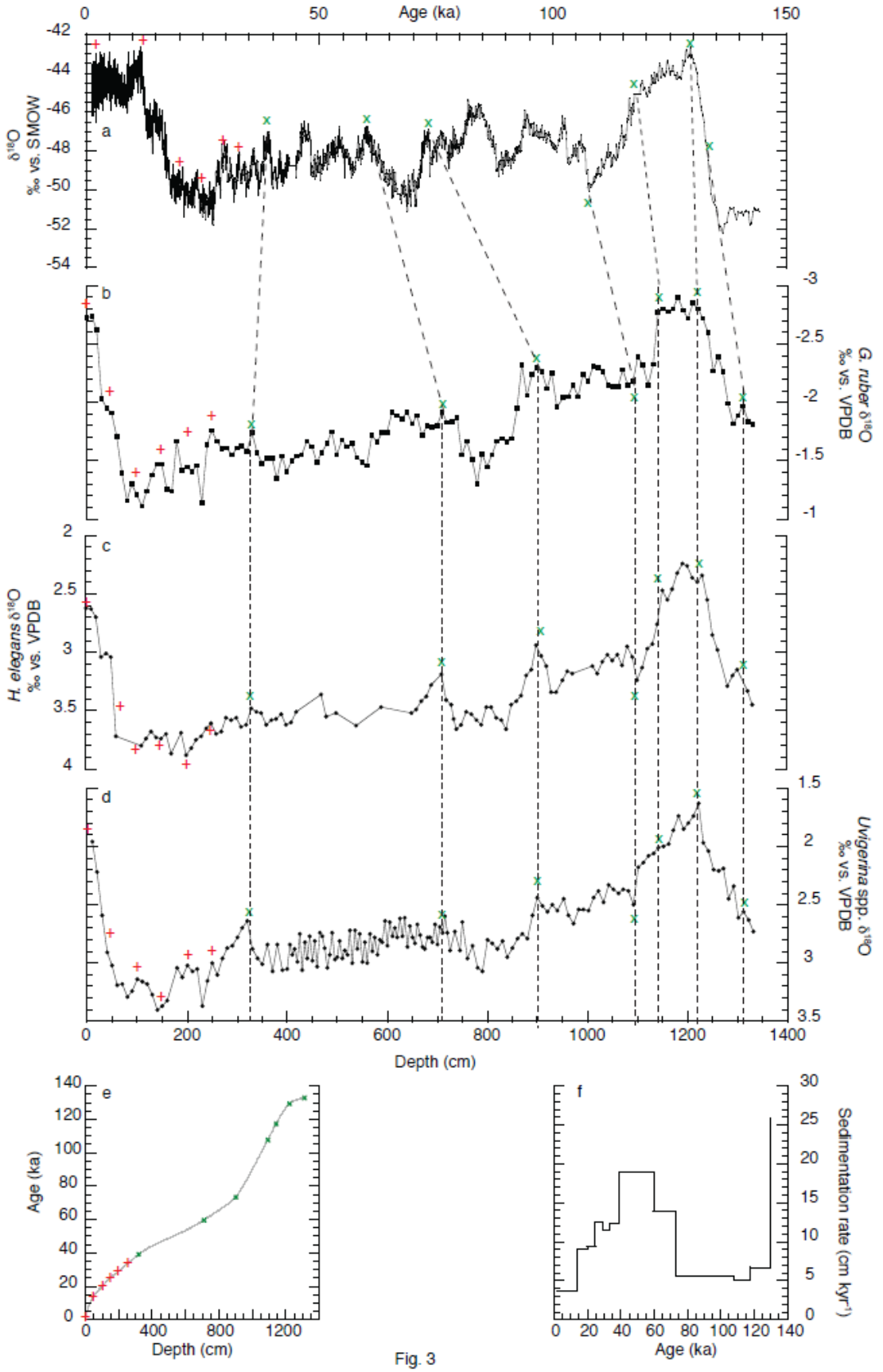

Fig. 3

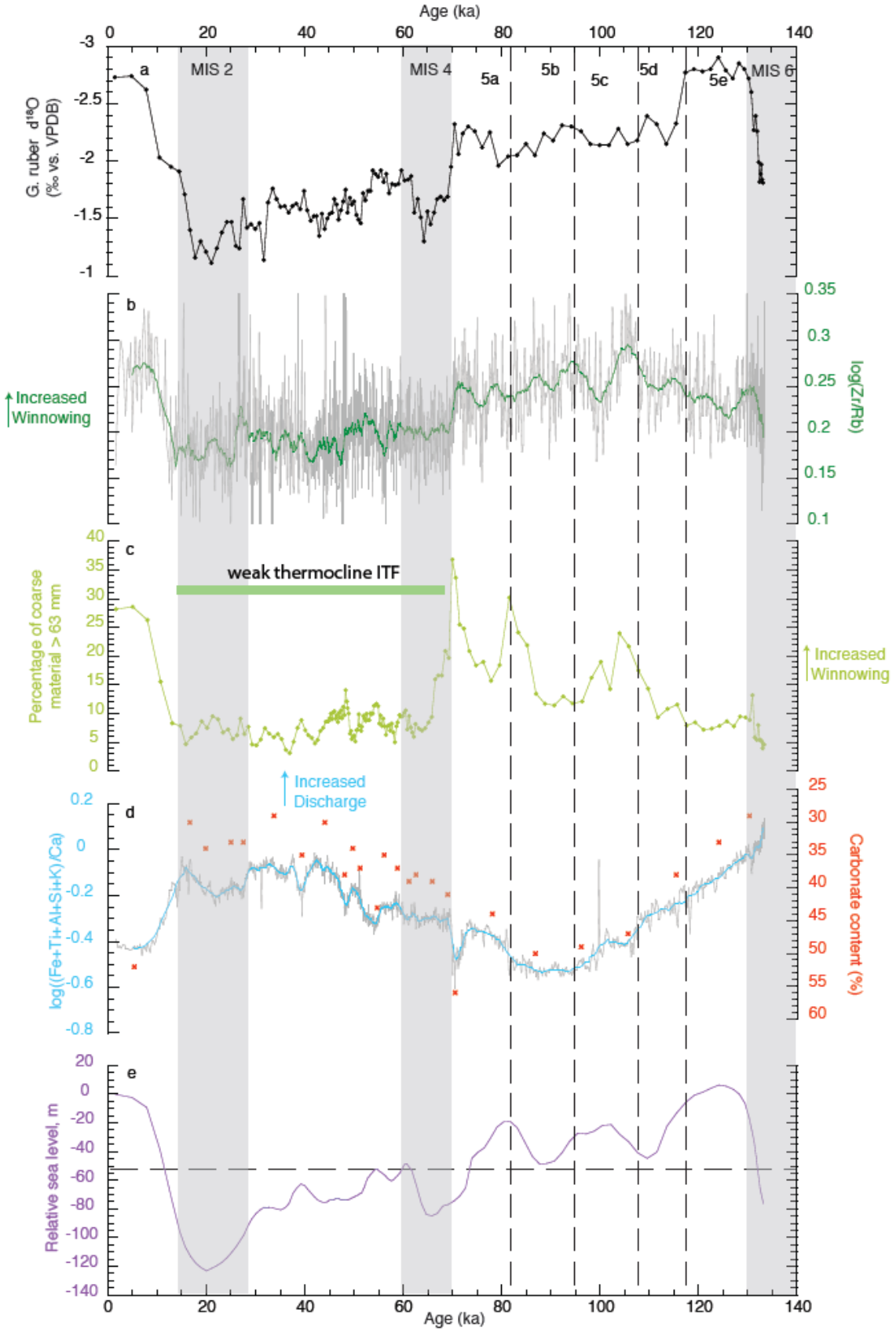

Fig. 4

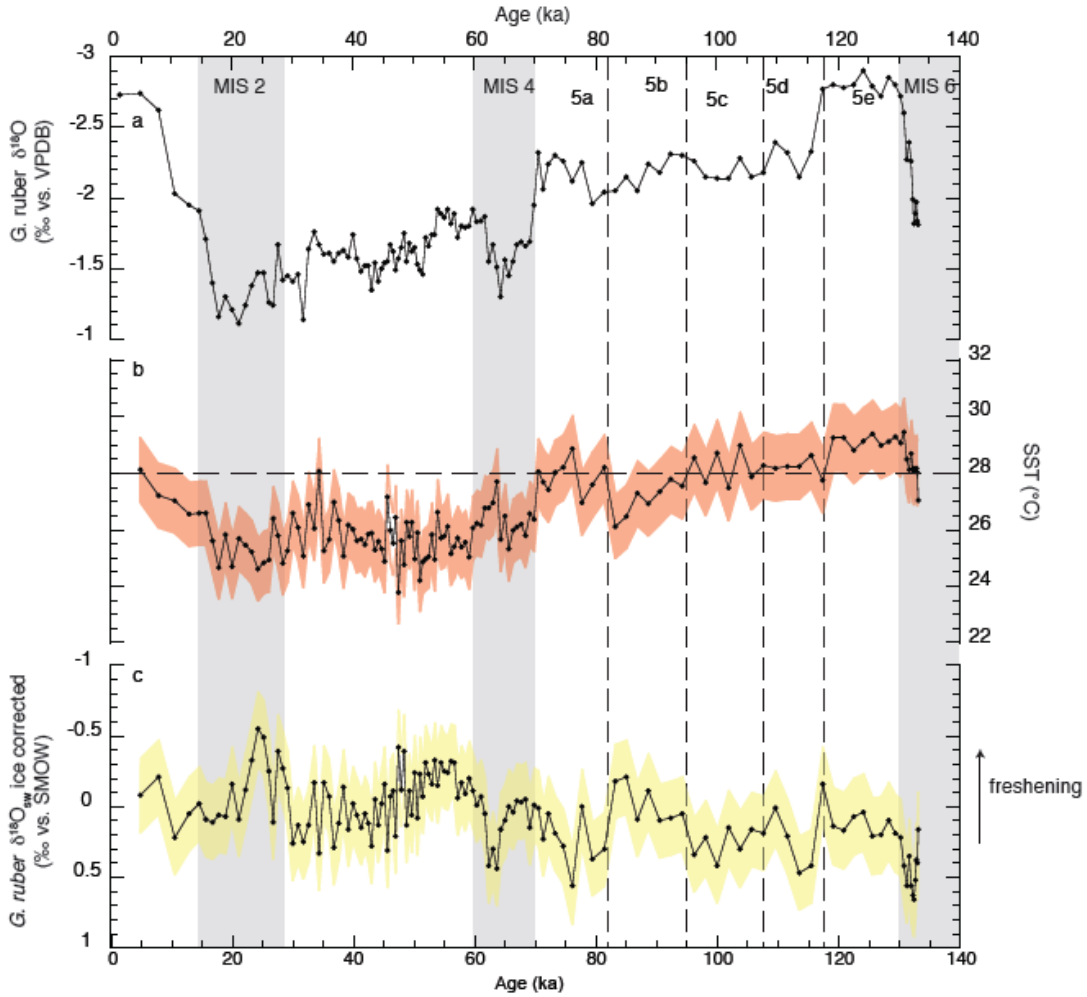

Fig. 5

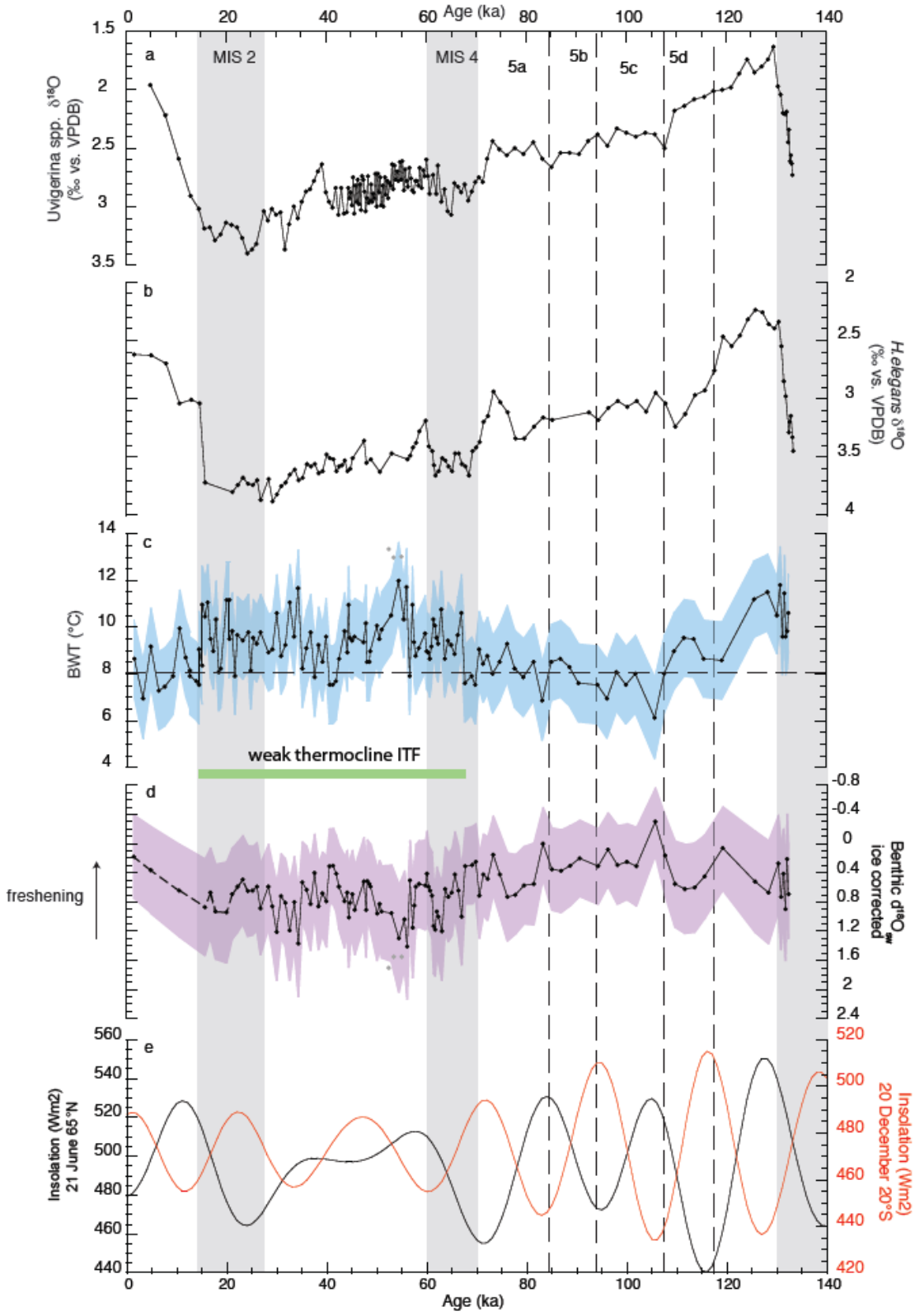

Fig. 6

Table 1. AMS ^{14}C dates and $\delta^{18}O$ events between sediment core SO18471 and the EDML-1 ice core (AICC2012)*.

Analysis	Sample (core SO18471)	Conventional ^{14}Cage, ka	Tie point	Calendar Age, ka	Species analyzed
AMS ^{14}C date	section I; 0-1 cm	1.745±25		1.4960**	*G.ruber*
AMS ^{14}C date	sectionI; 44-45 cm	12.280±80		13.950**	*G.ruber, G. sacculifer*
AMS ^{14}C date	section II; 100-101 cm	16.760±90		20.011**	*G.ruber*
AMS ^{14}C date	section II; 144-145 cm	20.790±180		24.816**	*G.ruber; G. sacculifer*
AMS ^{14}C date	section III; 200-201 cm	25.320±220		29.18**	*G.ruber*
AMS ^{14}C date	section III; 250-251 cm	29.560±420		33.525**	*G.ruber*
Foraminiferal ^{18}O	section IV; 320-321 cm		lowest ^{18}O value of A1	39.181*	*G.ruber ; H. elegans; Uvigerina* spp.
Foraminiferal ^{18}O	section VIII; 710-711 cm		lowest ^{18}O value of A4	59.748*	*G.ruber ; H. elegans; Uvigerina* spp.
Foraminiferal ^{18}O	section X; 900-901 cm		lowest ^{18}O value of MIS 5a	73.334*	*G.ruber ; H. elegans; Uvigerina* spp.
Foraminiferal ^{18}O	section XII; 1092-1093 cm		peak of MIS 5d	107.69*	*G.ruber ; H. elegans; Uvigerina* spp.
Foraminiferal ^{18}O	section XII; 1142-1143 cm		end of MIS 5e ^{18}O plateau	117.49*	*G.ruber ; H. elegans; Uvigerina* spp.
Foraminiferal ^{18}O	section XIII; 1222-1223 cm		onset of MIS 5e ^{18}O plateau	129.46*	*G.ruber ; H. elegans; Uvigerina* spp.
Foraminiferal ^{18}O	section XIV; 1312-1313 cm		midpoint of Termination II	132.93*	*G.ruber ; H. elegans; Uvigerina* spp.

*Veres *et al*., (2013)

**Calibration version for ^{14}C dates: IntCal13